The 5th International Symposium – Supercritical CO2 Power Cycles
March 28-31, 2016, San Antonio, Texas

Use of 1-D Finite Enthalpy Method for a High-Temperature Recuperator Made of Polymer Derived Ceramic Composite for a Supercritical Carbon Dioxide Power System

Mahmood Mohagheghi [1], Husam Zawati [1], Thomas Pinol [2], Jihua Gou [1], Chengying Xu [3], Jayanta Kapat [1]

1 Laboratory for Cycle Innovation and Optimization
Center for Advanced Turbomachinery and Energy Research (CATER)
University of Central Florida, Orlando, Florida, USA.
2 School of Engineering in Physics, Applied Physics, Electronics & Materials Science,
Grenoble Institute of Technology, Grenoble, France.
3 Florida State University, Tallahassee, Florida, USA.

ABSTRACT

This paper introduces and provides an assessment of finite enthalpy method (FHM) for design and computational analysis of microchannel heat exchangers (MCHEs). These heat exchangers are utilized to increase the overall efficiency of a recompression recuperated cycle (RRC) in a supercritical carbon dioxide (S-CO2) power system. Overall cycle parameters and heat exchanger heat loads are obtained through a cycle optimization process that has been described in prior research. The focus of this paper is to introduce FHM, a class of novel material called Polymer Derived Ceramic Composite (PDCC) and associated manufacturing for fabrication of these heat exchangers. The PDCC selected for this work limits the maximum temperature in the recuperators to 1450 ℃ (1723 K). However, in this paper, this temperature is limited to 923 ℃ (1196 K) in order to be consistent with other affiliated component development efforts. The design is implemented using a one-dimensional energy based discretization, with the heat transfer per segment being equal while the length of each segment is allowed to vary as necessary. Significant variations in thermodynamic properties of the working fluid make the energy based discretization preferred over the finite volume method for calculations. Counter-flow passages with square cross-sectional configuration are considered with restrictions imposed by material and manufacturing. A unique heat exchanger configuration called “stair-step”, introduced in earlier publications, is utilized for these heat exchangers. The properties of the S-CO2 are obtained using a Matlab code that reads from REFPROP and the log mean temperature difference (LMTD) for each element is calculated along with the pressure drops.

The low temperature and high temperature recuperators (LTR, HTR) in this study feature lengths of 0.899 and 1.88 m. The maximum relative pressure drop across the LTR and the HTR are calculated to be 35 and 79 KPa, respectively. Stress analysis is done on the low temperature recuperator and the results do not indicate structural failure.

INTRODUCTION

The use of supercritical carbon dioxide as a working fluid in power cycles has recently attracted much attention in the power generation industry. The S-CO2 Brayton Cycle could promote the advancements in nuclear, solar and waste heat recovery systems. As discussed by Feher, the benefit of using carbon dioxide as opposed to other fluids is the moderation value of its critical pressure, its stability and relative inertness for the temperature range of interest, non-toxicity and low cost operation [1]. Additional key advantage discussed by Dostal, is the high density of the fluid, which plays a role in reducing the scale of the turbomachine to a miniscule size [2]. Figure 1 shows a comparison between steam, helium and CO_2 turbines with their respective power output and size. As can be seen from the figure, significant reduction in size, and hence in capital cost, may be realized for S-CO2 turbines as compared to steam turbines. However, as indicated in table 1, one needs to focus on the entire balance of plant in order to make economic analysis (which is outside of the scope of this paper). In particular, one needs to consider manufacturing and cost of recuperation heat exchangers in order to make an overall economic assessment of S-CO2 power systems.

The thermodynamic properties of carbon dioxide proves to be a key to the overall cycle design. With the supercritical point being at 304.25 K and 7.39 MPa, the fluid transitions to a supercritical state at about room temperature. When at supercritical state, CO_2 allows heat rejection while maintaining the gaseous state that flows through the expander and thus produces work using the design methods of gas and steam turbines. The main advantage of the supercritical CO_2 cycle is the increase of efficiency. Due to the fluid's density, the size of component for producing a comparable power outputs system is reduced, therefore resulting in an overall lower capital cost.

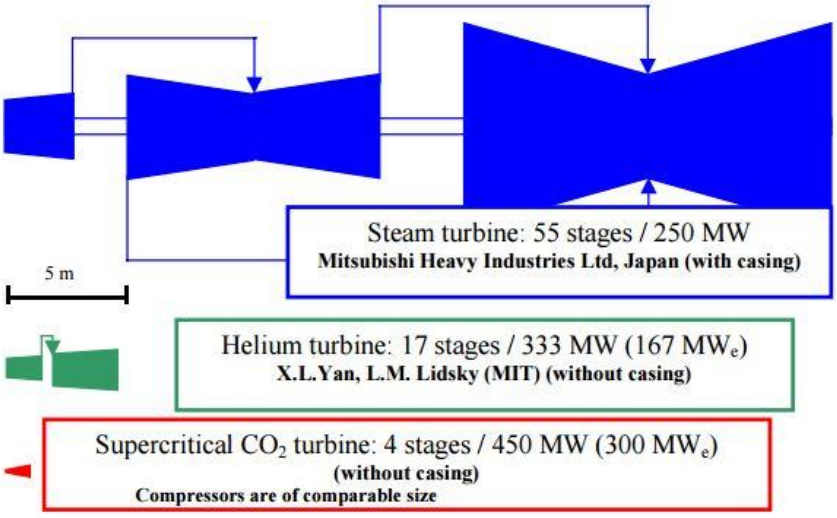

FIGURE 1: STEAM, HELIUM AND CO_2 TURBINE SIZE COMPARISON [2]

TABLE 1: MAIN COMPONENTS OF STEAM AND S-CO_2 TURBINES

	Steam Rankine Cycle	S-CO2 Brayton Cycle
Drive of working fluid	Pump	Compressor(s)
Main heating source	HRSG/boiler	Nuclear/solar/transportation/…
Recuperation system	N/A	LTR and HTR
Cooling system	Once through/wet tower/dry cooling	Coolers

MATERIAL AND MANUFACTURING BACKGROUND

Polymer Derived Ceramic Composites (PDCCs) are composite materials that start as a polymer composite and then can be converted to ceramic composite for high temperature parts and components. They exhibit creep resistance for up to remarkably high temperatures [3-6]. Since the fabrication process starts from liquid resin precursor like any other polymer composite (figure 2), the fabrication process can be inexpensive, except for the cost of fibers depending on the one selected. Complex shapes can be formed using existing techniques. Despite their endurance for temperatures of up to $1450\ °C$ [8-10], one major handicap of making the material is the brittleness of ceramics. However, this brittleness is somewhat compensated by use of fibers. The various resins considered for this study are listed in table 2. SMP-10 is selected for its higher temperature capability. The various ceramic fibers considered for this study are listed in table 3. From this, Nextel 720 and Hi-Nicalon (Type S) are selected for low and high temperature applications, respectively.

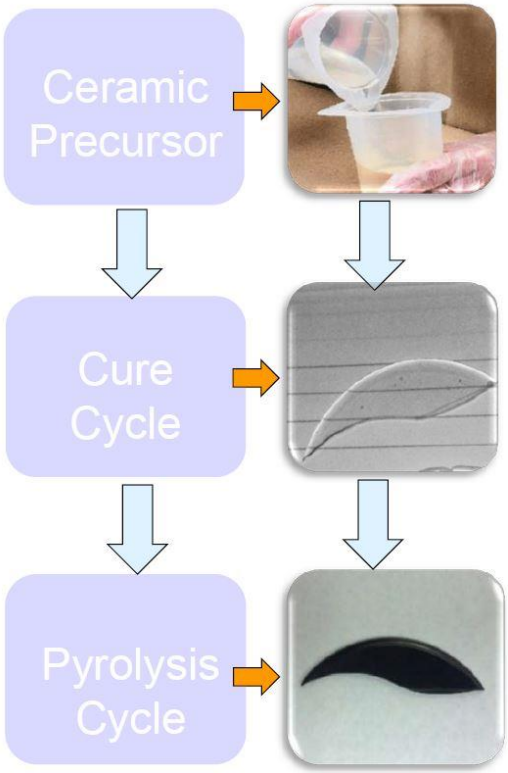

FIGURE 2: PROCESS STEPS FOR PDCC [7]

TABLE 2: PROPERTIES OF PDCC RESINS [7]

	SPR-688	SMP-10
Density (g/cm^3)	1.11	0.998
Viscosity ($mPa.s$ at 25°C)	300-2000	40-100
Flash point (°C)	93	89
Operating temperature (as ceramic) (°C)	1100	1800

TABLE 3: HIGH TEMPERATURE CERAMIC FIBERS [7]

Trade-Name	Manufacturer	Use temperature	Cost ($/kg)	Filament diameter (μm)	Density (g/cm^3)	Tensile strength (MPa)	Tensile modulus (GPa)	Composition	Thermal expansion (Ppm/℃)
T300	Toray	300~350 ℃	68	7	1.74	3100	230	C	-0.7
Nextel 720	3M	1204 ℃	660	10~12	3.4	2930	260	Al_2O_3/SiO_2	6
SCS-Utra	Specialty Material	1371 ℃	~9000	142	3.08	3900	380	SiC	4.1
SiC-1900X	MATECH	~1482 ℃	-	10~12	3.14	2500	367	β-SiC	-
Nicalon NL-200	Nippon Carbon	1100 ℃	~2000	14	2.55	3000	220	SiC	3.1-3.2
Hi-Nicalon	Nippon Carbon	1230 ℃	8000	14	2.74	2800	270	SiC	3.3-3.5
Hi-Nicalon (Type S)	Nippon Carbon	1450 ℃	13000	12	3.1	2600	420	SiC	3.5
Sylramic	COI Ceramics	1420 ℃	10000	10	3.55	3200	380	SiC	5.4
Tyranno SA 1-3	Ube Industries	1700 ℃	5000	10	3.02	2800	375	SiC	-

There are multiple steps of producing a continuous fiber reinforced ceramic matrix composite. Polymer Infiltration and Pyrolysis (PIP) involves an infiltration of a low viscosity polymer resin precursor into a ceramic fabric (figure 2). Once wet lay-up is completed, a cure cycle (of ramp up, hold and ramp down) is performed inside an autoclave (figure 3 left) without oxygen in order to obtain polymer composite structure. Then a pyrolysis cycle is used inside a kiln (figure 3 right) with temperature up to 1000 ℃ in order to remove polymer chain, thus leaving behind ceramic backbone. Up to 8% shrinkage may happen in this process.

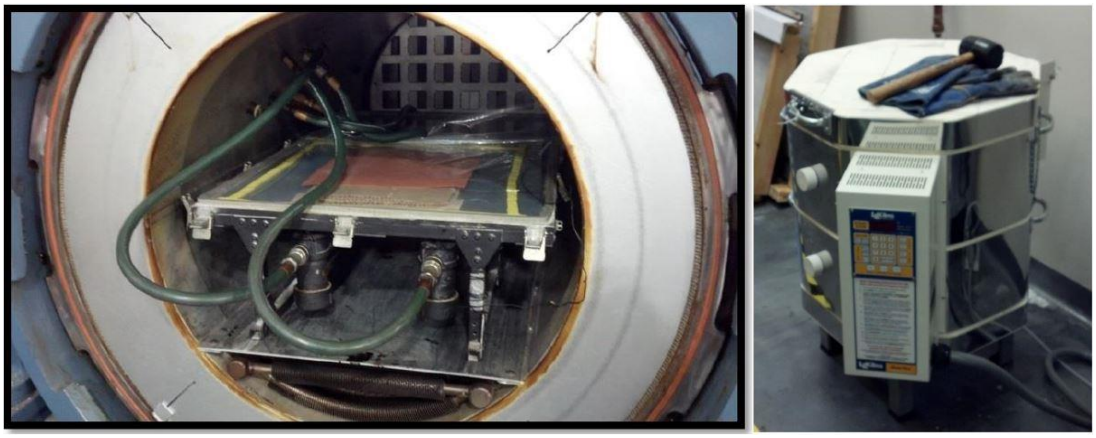

FIGURE 3: AUTOCLAVE FOR CURE CYCLE (LEFT) KILN FOR PYROLYSIS (RIGHT) [7]

Reinfiltration with the polymer and further pyrolysis cycles are required to increase the density of the ceramic matrix. Thus, the ceramic content and the strength of final product are increased. Oxyacetyline torch testing (ASTM E285) (figure 4), and 3-point bend testing (ASTM C1341) are used to obtain some of the thermal and mechanical properties of manufactured panels. So far, only flat panels have been manufactured as part of this study.

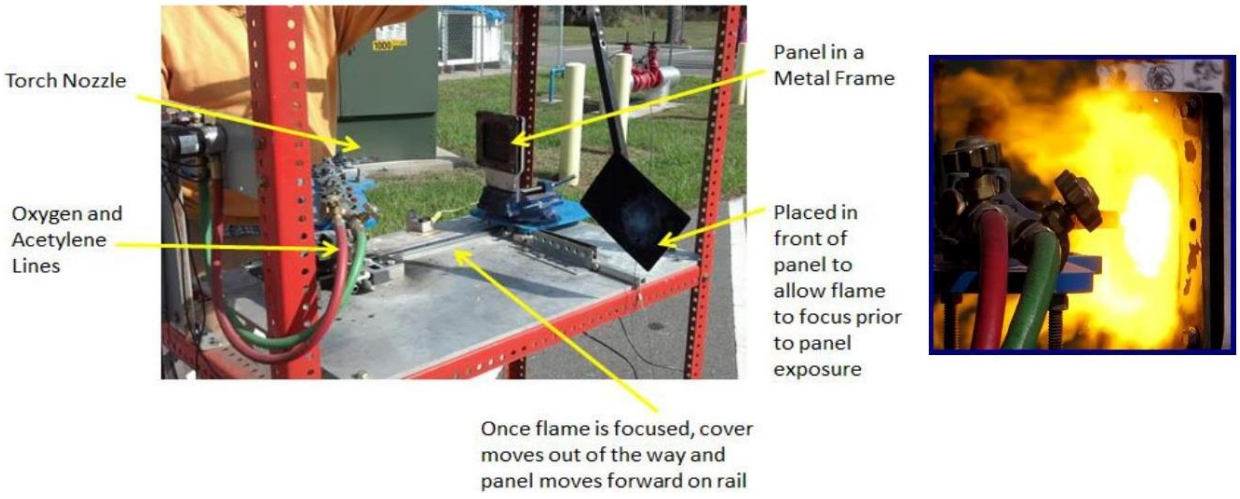

FIGURE 4: OXYACETYLENE TORCH TESTING [7]

METHODOLOGY

The 1-D FHM used in this study is coded in Matlab. A Genetic Algorithm (GA) is used to minimize the weight of heat exchanger cores while keeping the relative pressure loss values less than or equal to the ones assumed in the cycle calculations [11]. The first iteration then begins with the first value of decision variables that consist of the hydraulic diameter and the total number of channels in the heat exchangers. Based on the initial

values of the decision variables, the performance indicators such total length, the mass of the heat exchanger and the relative pressure loss are calculated. The process is repeated for several iterations until the criteria of the objective function is satisfied.

Cycle Calculations

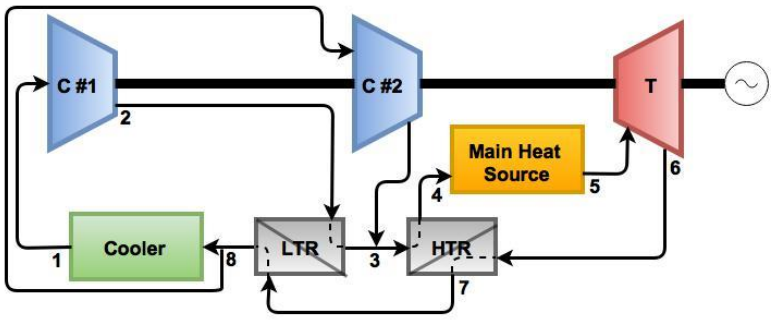

FIGURE 5: RECOMPRESSION RECUPERATED CYCLE

Figure 5 represents a diagram of an RRC cycle. The flow exiting the main heat source gains the necessary heat to reach the turbine inlet temperature, then goes through the HTR, LTR and splits into two streams at point 8; main fraction of the mass flow ($frac_{main}$) goes to the main compressor while the rest goes to the second compressor to undergo a recompression process. Both flows meet up again in point 3 before entering the HTR. The numbers on the diagram will be used as a reference throughout this paper. Table 4 compares performance parameters for the main compressor (C #1) and the secondary compressor (C #2).

TABLE 4 : MAIN COMPRESSOR AND RECOMPRESSION PERFORMANCE PAREMETERS

	Main Compressor (C #1)	Recompression (C #2)
Total mass flow rate (kg/s)	660.405	
Mass flow fraction ($frac$)	0.715	0.285
Mass flow (kg/s)	472.19	188.215
Intake power (kW)	179389	14504.6

This study focuses on a 100MW net power RRC S-CO2 Brayton cycle power system, with a maximum pressure of 24MPa and a turbine inlet temperature of 1350 K. Overall cycle efficiency is found to be 59.11% and the mass flowrate for the working fluids is 660.405 kg/s. The cycle state points are presented in table 5 and shown on the T-S diagram of figure 6.

TABLE 5: STATE VALUES FOR S-CO2 BRAYTON CYCLE

Point	T (K)	P (kPa)	h(kJ/kg)	ρ (kg/m^3)	s ($kJ/kg.K$)
1	320	9500	382.5	374.3	1.579
2	378.9	24000	420.5	544.2	1.599
3	487.9	23976	606.8	295.8	2.035
4	1154.4	23952	1455.6	103.8	3.134
5	1350	23904.1	1713	88.6	3.34
6	1196.6	9691.2	1511.8	41.9	3.359
7	498.2	9643	662.9	109.3	2.305
8	388.9	9595	529.7	162.7	2.003

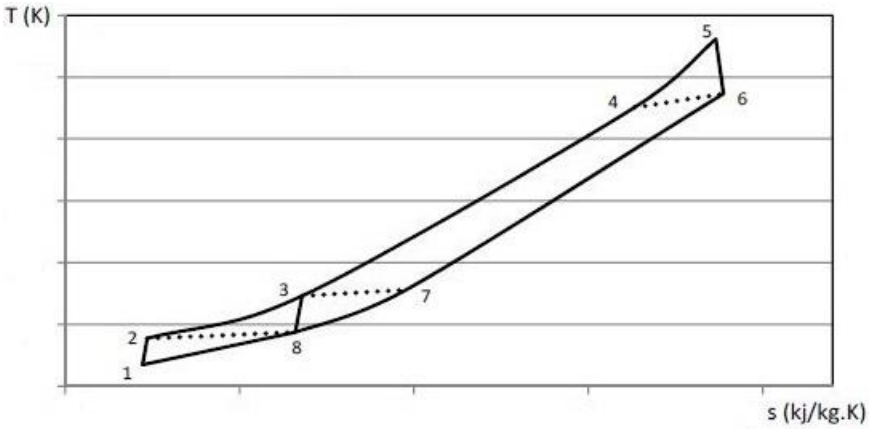

FIGURE 6:T-S DIAGRAM OF RRC CYCLE

Concept

The design of interest in the MCHEs is the counter flow heat exchangers, formed of PDCC. Plates are bonded at a 45 degree angle to form squared channels as shown in figure 7. Thickness of channel walls is set at 0.35 mm, hydraulic diameter and the number of channels are determined through the GA iterative process.

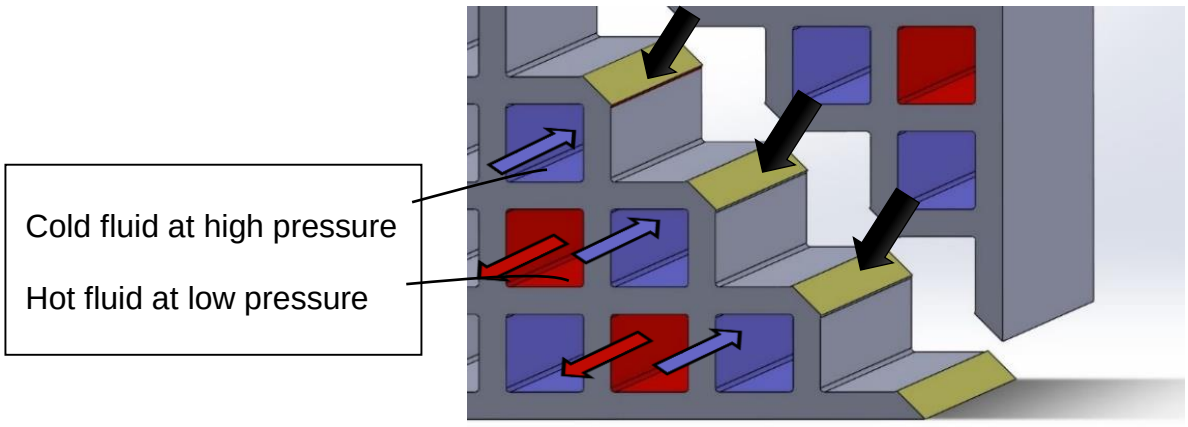

FIGURE 7: PDCC FORMING MICROCHANNELS

Figure 8 shows a conceptual solid model design of a MCHE with 36 channels was studied by Schmitt, Amos and Kapat [12]. The heat exchanger shown illustrates how the squared channels are formed together. Figure 8 (a) shows a cross sectional area of the headers in the heat exchanger, while figure 8 (b) shows the hot and the cold fluid entrance and exit. The inside of the heat exchanger is made of plates shown in figure 8 (right), as the fluid advances it faces the flat plate first then proceeds to the 'stepped' configuration so that towards the middle body, the cross sectional view would look like figure 8 (c).

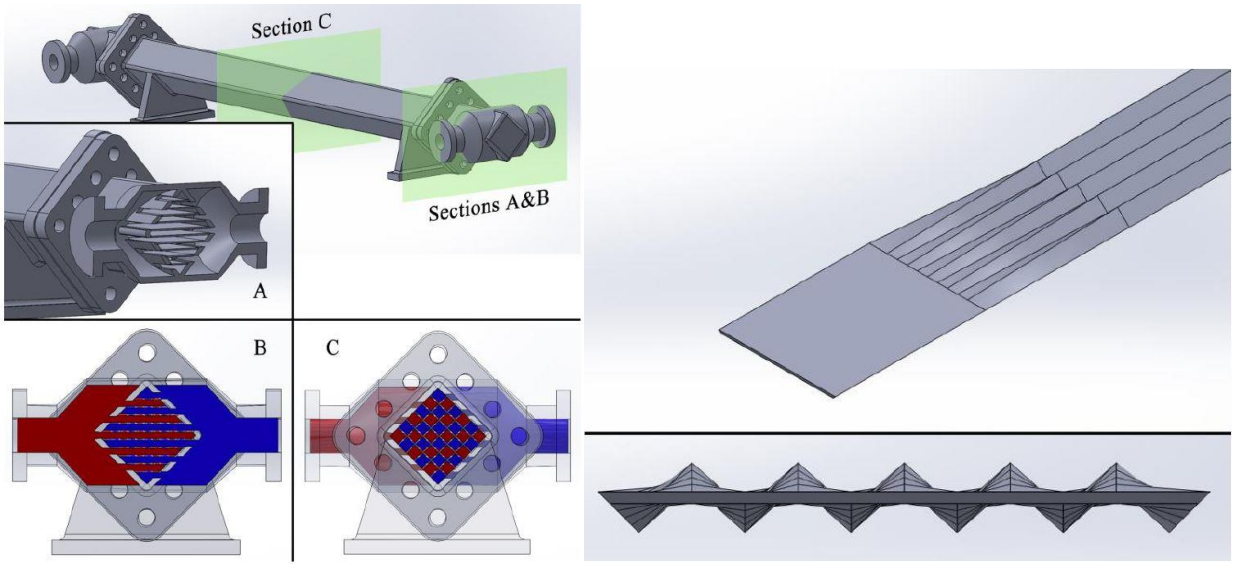

FIGURE 8: SECTIONS OF A CONCEPT MICROCHANNEL HEAT EXCHANGER WITH FLUID VISUALIZATION (LEFT), CHANNEL TRANSITION FROM STEP TO FLAT (RIGHT) [12]

High Temperature Recuperator

The HTR used between points (3, 4, 6, 7) transfers heat from the Low Pressure (LP) fluid exiting the turbine (points 6, 7) to the high pressure (HP) fluid (cold fluid). The mass flow rate for the high and low pressure fluids are equal and can be calculated as:

$$\dot{m}_{HTR} = \frac{Net\ Output}{Specific\ Power} = \frac{100\ MW}{W_t - (W_{C1} + W_{C2})} \qquad (1)$$

$$= \frac{100\ MW}{((h_5 - h_6) - ((h_2 - h_1) frac_{main} + (h_3 - h_8)(1 - frac_{main}))} \qquad (2)$$

Heat load is defined as:

$$\dot{Q}_{tot\ HTR} = -\dot{m}_{HTR} \,.\, \Delta h_{LP} = \dot{m}_{HTR} \Delta h_{HP} \qquad (3)$$

Low Temperature Recuperator

Between points (2,3,7,8), fluid exiting main compressor at point (2) is heated to point (3) by the LP fluid exiting the HTR (7,8) in order to be mixed with the fluid exiting the

second compressor (point 3). Therefore, the LP and HP mass flow rates in the LTR are different (points 8, 9).The mass flow rates and heat loads are:

$$\dot{m}_{LTR_{LP}} = \dot{m}_{HTR} \quad (4)$$

$$\dot{m}_{LTR_{HP}} = frac_{main}.\dot{m}_{HTR} \quad (5)$$

$$\dot{Q}_{tot_{LTR}} = -\dot{m}_{LTR_{LP}}.\Delta h_{LP} = \dot{m}_{LTR_{HP}}.\Delta h_{HP} \quad (6)$$

Design by Iterations

Calling properties from REFPROP [13] database is time consuming and obtaining results will be hard to achieve without the use of the GA. Using REFPROP, a pre-defined ranges of temperatures and pressures (table 6) are used to obtain values of specific heat, density, Prandtl number, thermal conductivity and dynamic viscosity. Those values are stored in a file and bi-linear interpolation is used to obtain the values needed.

TABLE 6: PRE-DEFINED TEMPERATURE AND PRESSURE VALUES

	Range	Resolution	# of values
Temperature	$300 < T < 1500\ K$	$1\ K$	1200
Pressure	$7 < P < 25\ MPa$	$0.05\ MPa$	360

Since the length of the MCHE is assumed to be much larger than the hydraulic diameter, both high and low pressure fluids are assumed to be fully developed. Input parameters are the pre-defined values that are obtained either through cycle calculations or previous knowledge of manufacturing limits. Those parameters are used to start the first iteration in order to calculate the correlations found in table 8 for every discretized element. Design/decision variables can be defined as the set of values that are calculated and iterated until the optimum design point is achieved. Table 7 shows the input parameters and decision variables for the design of the MCHE.

TABLE 7: INPUT PARAMETERS AND DECISION VARIABLES

Input Parameters		
Geometry	Channel thickness	t
LP and HP fluids	Inlet and outlet temperature (K)	$T_{L/HP_{in}}, T_{L/HP_{out}}$
	Inlet and outlet pressure (kPa)	$P_{L/HP_{in}}, P_{L/HP_{in}}$
	Mass flow rate (kg/s)	$\dot{m}_{L/HP}$
Decision Variables		
Geometry	Hydraulic Diameter	D_h
	# of channels	$n_{channels}$
	# of elements	n_e

Each channel is divided into a number of elements along the length and each element has an equal amount of heat transferred. Because the quantity of properties change along the channel while the heat transferred is equal, the length of each of those

elements change to maintain the same heat transfer per element. A thermal resistance model is utilized through the walls to represent the conduction heat transfer and is shown in figure 9, where the thermal conductivities and Nusselt numbers are calculated in the middle of each element.

The length of the elements are found through 1-D calculations using the LMTD method and the final length of the MCHE is obtained through adding the length of the elements obtained using the discretization method. The equations used in the iterative process are summarized in table 8.

Heat Transfer through the wall and between the fluids is represented by a thermal resistance in series for each of the elements. Nusselt numbers and the thermal conductivities for the material are calculated at the middle point of the element. The material is assumed to be isotropic and therefore the wall resistance is constant all through the length.

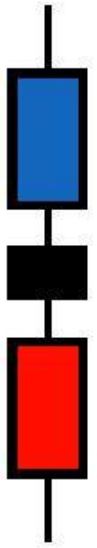

$$h_{convHP} = Nu_{HP} . \frac{k_{HP}}{d} \quad (7)$$

$$R_{wall} = \frac{t}{k_{cross}} \quad (8)$$

$$h_{convLP} = Nu_{LP} . \frac{k_{LP}}{d} \quad (9)$$

FIGURE 9: HEAT TRANSFER RESISTANCE MODEL ACROSS TWO CHANNELS

The equations in table 8 below are utilized “j” times until the convergence to a final length is reached. The mass flow rate (equations 1, 4) are found and used in equations (3, 6) to find the total heat load. Then, the heat per element (equation 10) is calculated to be used in equation 12, to find the temperature of each element. This value is then used to calculate the average temperature at the middle of the element (equation 11) and is used to find the LMTD (equation 13). The velocity, Reynolds number, Darcy friction factor, Nusselt number as well as the overall heat transfer coefficient (equations 14-21) are then used to find the length of each element (equation 22). Finally, the pressure drop across the element is calculated through the Darcy-Weisbach equation 23.

TABLE 8: CORRELATIONS AND EQUATIONS FOR THE ITERATIVE PROCESS

Property	Equations & Correlation	
Heat per element (W)	$\Delta\dot{Q} = {\dot{Q}}/{n}$	**10**
Average temperature for jth iteration	$T_{H\backslash LP\,avg}(i-1) = \frac{1}{2}T_{H\backslash LP_j}(i-1) + \frac{1}{2}T_{H\backslash LP_{j-1}}(i)$	**11**
Temperature (K)	$T_{H\backslash LP}(i) = T_{H\backslash LP}(i-1) + \frac{\Delta\dot{Q}}{\dot{m}_{H\backslash LP}C_{p\,H\backslash LP}(i-1)}$	**12**
LMTD (K)	$LMTD(i) = \frac{\left((T_{LP}(i) - T_{HP}(i)\right) - (T_{LP}(i+1) - T_{HP}(i+1))}{\ln(\frac{T_{LP}(i) - T_{HP}(i)}{T_{LP}(i+1) - T_{HP}(i+1)})}$	**13**
Velocity (m/s)	$V = \frac{\dot{m}}{\rho.s}$	**14**
Reynolds number	$Re = \frac{\rho V D_H}{\mu} = \frac{\dot{m} D_H}{\mu.s}$	**15**
Darcy friction factor	$f_D = \frac{64}{Re}$	**16**
	$\frac{1}{\sqrt{f_D}} = -2\log(\frac{\varepsilon}{3.7D_H} + \frac{2.51}{Re\sqrt{f_D}})$	**17**
Nusselt number	$Nu = 3.61$	**18**
	$Nu_D = \frac{\left(\frac{f_D}{8}\right)(Re_D - 1000)Pr}{1 + 12.7\sqrt{\frac{f_D}{8}}(Pr^{2/3})}$	**19**
Heat transfer coefficient ($^{W}/_{m^2.K}$)	$h = Nu\frac{k_{fluid}}{D_H}$	**20**
Overall heat transfer coefficient	$U = \frac{1}{\frac{1}{h_{LP}} + \frac{1}{h_{HP}} + \frac{t}{k}}$	**21**
Δx (m)	$\Delta x(i) = \frac{\Delta\dot{Q}}{4D_H\,LMTD(i)U(i)}$	**22**
Pressure loss	$dP(i) = 0.5\rho f_D \Delta x(i)\frac{V^2}{D_H}$	**23**

To reach a grid convergence, the number of elements was chosen at a point where the length of the channel stops changing. Figure 10 below shows the flow chart representing the calculation process for a single iteration.

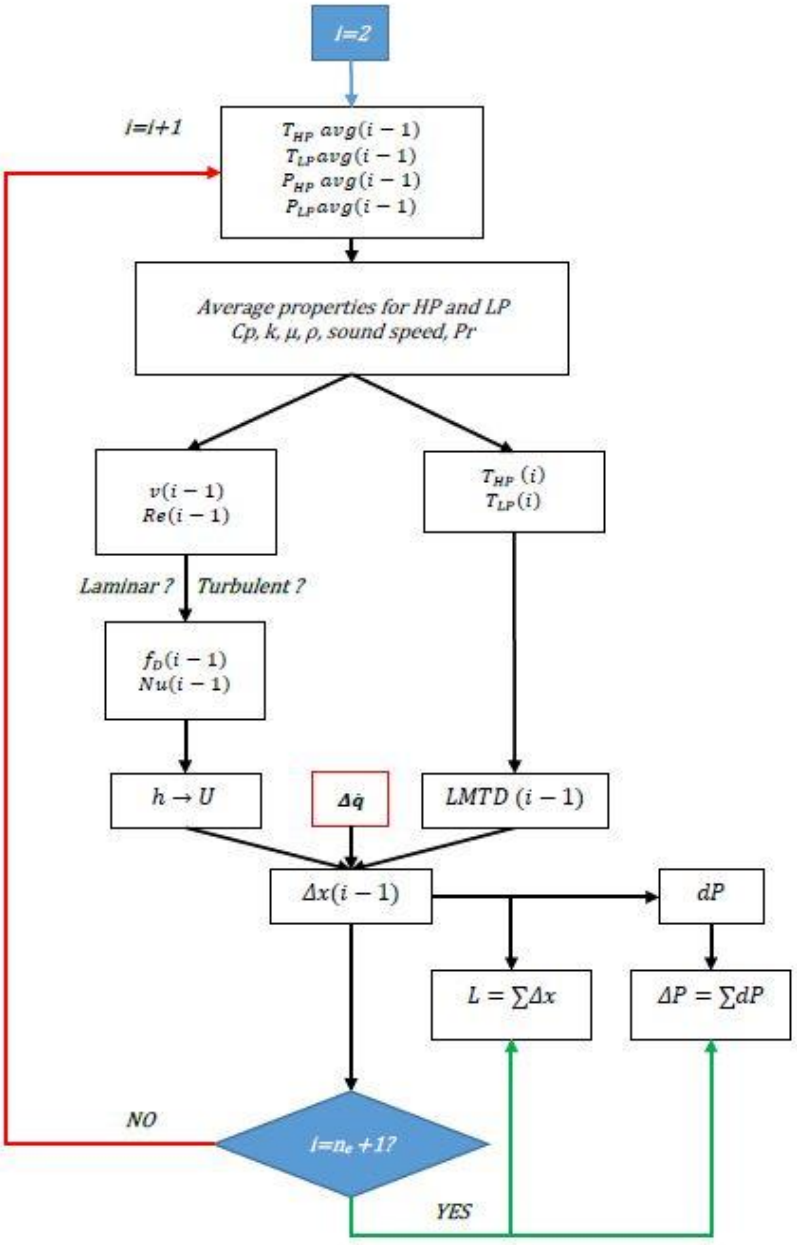

FIGURE 10: FLOW CHART PROCESS FOR A SINGLE ITERATION

RESULTS AND DISCUSSION

Results presented are based on a turbine inlet temperature of 1350 K. PDCC is chosen for the material of both LTR and HTR which results are presented below because it has the ability to endure the high pressure and temperature of the working fluid, as well as the resistance of corrosion and erosion. In comparison to the results obtained using

REFPROP, errors are within a 0.0001% window due to correlations and assumptions. Table 9 summarizes the MCHE dimension inputs and results.

TABLE 9: DIMENSION INPUTS AND RESULTS

$k_{cross}\ (^{W}/_{m.K})$		
$10^{-11}T^4 - 2 * 10^{-8}T^3 + 2 * 10^{-5}T^2 + 0.0104T + 5.7944$		
$k_{long}\ (^{W}/_{m.K})$	ε (m)	
5	$15x10^{-6}$	
MCHE dimensions		
	LTR	HTR
Hydraulic Diameter	1.003 mm	1.014 mm
t	0.35 mm	0.35 mm
$n_{channels}$	770	1107
Heat load	87.96 MW	560.59 MW
Mass flow rate	$\dot{M}_{LTR_{LP}} = 510.21\ ^{kg}/_{s}$ $\dot{M}_{LTR_{HP}} = 364.8\ ^{kg}/_{s}$	$\dot{M}_{HTR} = 510.21\ ^{kg}/_{s}$
n_e	580	700
Iterations	7	7
Length	0.89927 m	1.88 m
Width	2.08 m	3.02 m
Total mass	1757 kg	7676 kg

For the HTR, the element size decreases along the length of the MCHE. As the n^{th} element is approaching the LP inlet, the amount of heat needed to be transferred becomes less. Similarly, the element size for the LTR increases as it is going further away from the LP inlet. Since the element size for the LTR is increasing over the course of length in channel, the heat load curvature slope is becoming flatter whereas the HTR heat load slope is increasing since it is ruled by the increase of element length. Figure 11 shows the relationship between the heat load and length of channel for both LTR and HTR.

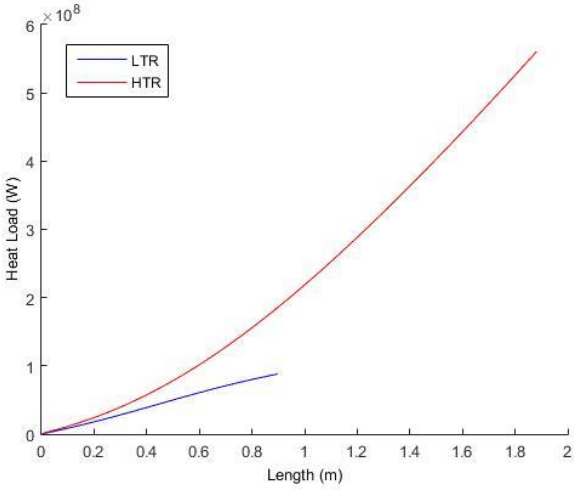

FIGURE 11: CHANGE IN HEAT LOAD FOR LTR AND HTR

Unlike air as a working fluid in an ordinary gas turbine, CO_2 undergoes huge thermodynamic variations in the region around its critical point. Figure 12 represents the change in specific heat across the length of the microchannels. The specific heat of the S-CO2 varies dramatically in this region and drops across the LTR. This influences the temperatures calculated in each of the elements, and this justifies the increase in temperature along the channels and the heat transfer.

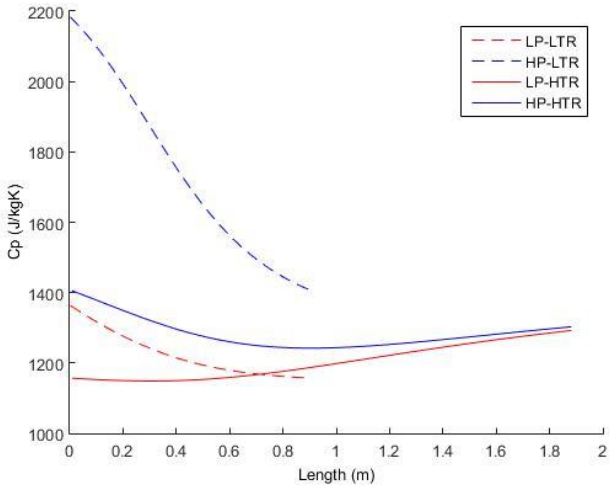

FIGURE 12: CHANGE IN SPECIFIC HEAT

Results for temperatures are summarized in table 10. Input values and cycle calculations presented in table 5 show a relative difference of <±1%.

TABLE 10: TEMPERATURE RESULTS FOR LTR AND HTR

	LTR	HTR
$T_{LP_{out}}$ (input)	373.4	468.6
$T_{HP_{in}}$ (input)	363.4	458.6
$T_{LP_{in}}$ (out)	468.3	817.6
$T_{HP_{out}}$ (out)	461.9	777.05

The heat load in the channels is a function of temperature of the inside and therefore, it is expected to see similar curvature slopes of temperatures along the length and the heat load as represented in figure 13.

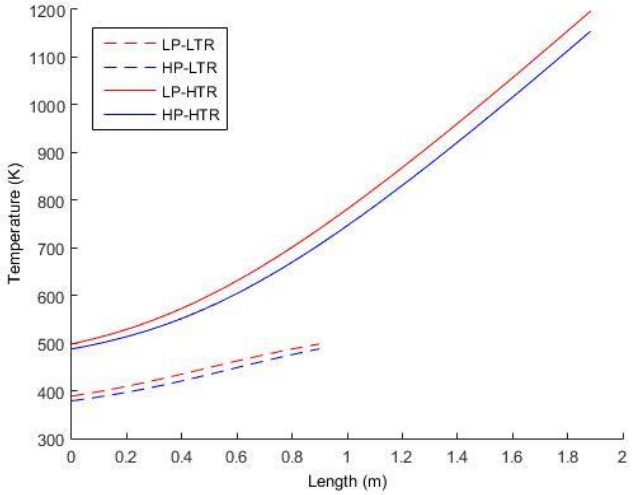

FIGURE 13: VARIATION IN TEMPERATURE

Pressure drops are calculated through the Darcy-Weishbach equation 23, which are caused because of the friction along the walls of the channels. The equation is valid for incompressible fluids, yet it provides a first approximation of pressure drop along the length of the MCHE. Table 11 shows a very close deviation between the calculated pressure from the cycle analysis and the iterative process.

TABLE 11: COMPARISON BETWEEN CALCULATED AND GIVEN PRESSURES

(MPa)	LTR	HTR
$P_{LP_{out}}$ (given)	10.366	10.418
$P_{LP_{in}}$	10.413	10.462
% difference	0.45	0.42
$P_{HP_{in}}$ (given)	24	23.88
$P_{HP_{out}}$	23.992	23.862
% difference	0.033	0.075

STRESS ANALYSIS

Stresses on the inner walls of the recuperators can be a design issue due to the high pressure exposures. The LTR discussed previously is studied for deflection and stresses along the inner walls of the recuperator. Due to computational constraints, the number of channels is greatly reduced to 100 while the length of is maintained at 50 times the channel's hydraulic diameter; about 5 cm. The material's properties are shown in table 12.

TABLE 12: MECHANICAL PROPERTIES OF PDCC

Poisson's ratio	0.225
Tensile Strength	$1.7\ GPa$
Young's Modulus (E)	$2\ GPa$

Density (ρ)	$2000\ (^{kg}/_{m^3})$
Thermal Conductivity (k)	$5\ ^{W}/_{m.K}$

The model used for the stress study is modeled in a CAD software package, then imported into the Static Structural module in Ansys Workbench 16.0 for further analyses. The pressures were assumed to not have a dropping gradient across the length of the channels and the faces constrained since the sample model is a fraction of the heat exchanger. Figure 14 shows the geometry preparation.

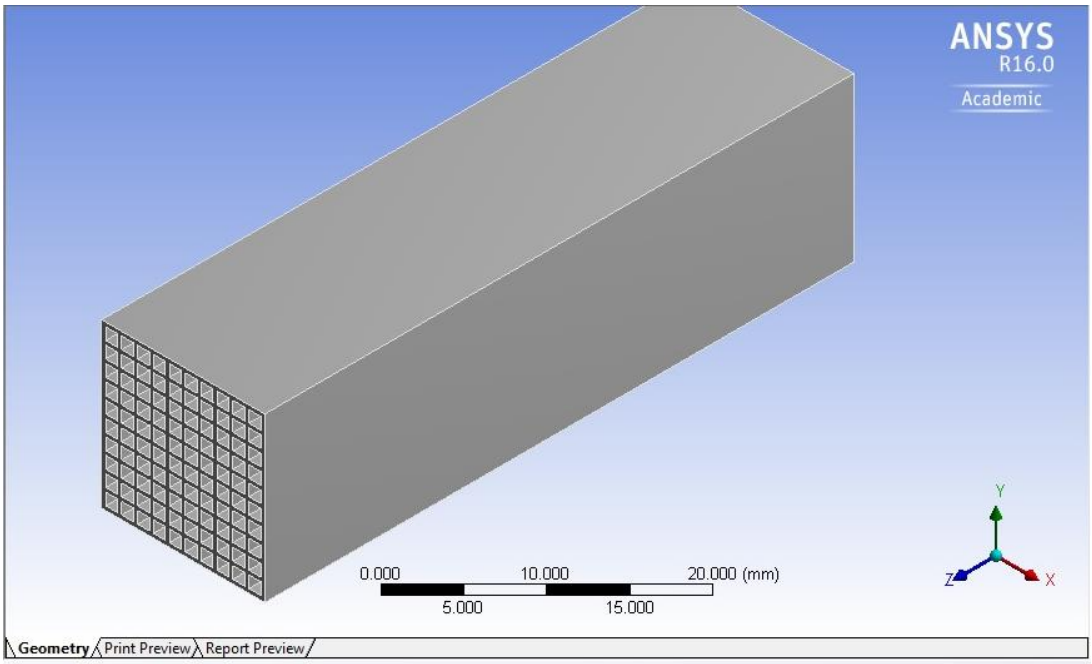

FIGURE 14: BINARY SOLID GEOMETRY RAW CAD

In order to prepare the solid body, a tetrahedron meshing was used over the volume, with a base size of 0.25 mm. While the channel wall thickness is consistent at 0.35 mm, which ensured the walls had enough elements to improve the precision of the results. Figure 15 shows the solid body after meshing with an overall statistics show results of approximately (2.6) million elements and (4.3) million elements.

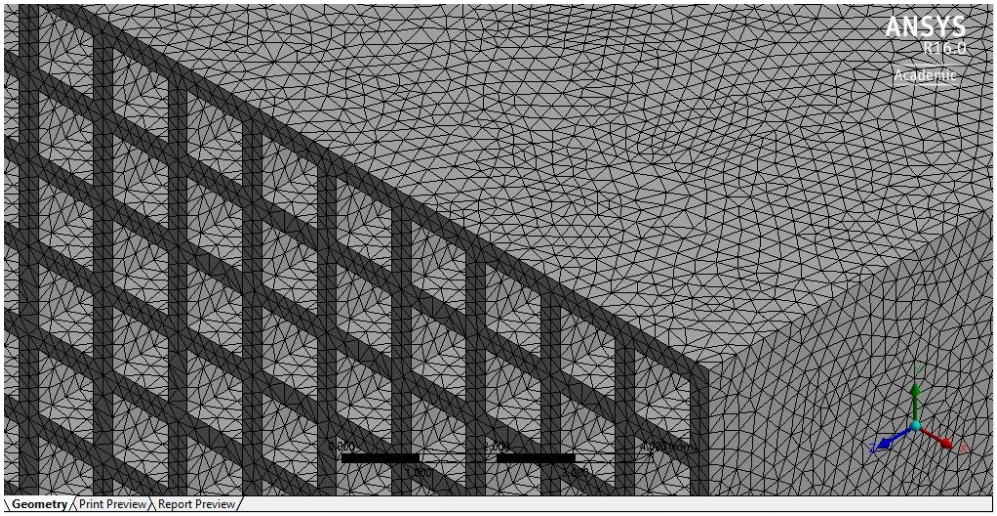

FIGURE 15: GEOMETRY TETRAHEDRON MESH

From the cycle calculations in table 5, inlet pressures for the recuperators are known. The same values are used to specify the constant pressure values on the inner walls of the recuperators. The LTR had a pressure inlet of 24 MPa and the HTR had a pressure inlet of 9.5 MPa. Figure 16 shows a visualization of the HP and LP fluids assigned in a checkers form.

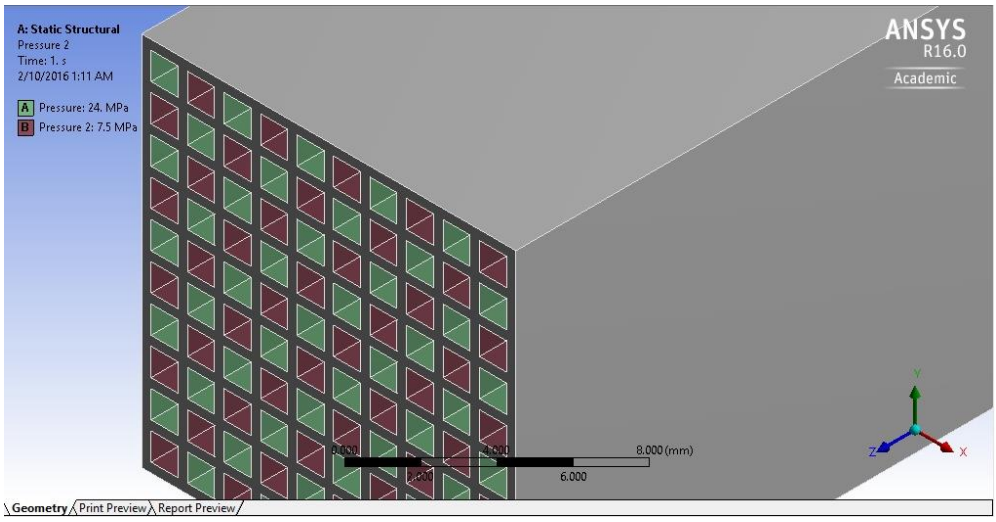

FIGURE 16: HIGH (GREEN) AND LOW (MAROON) PRESSURE REGIONS

Since the model of study is a part of a much larger geometry, the 6 sides of the model (4 sides and front/back faces) are constrained and assumed to be fixed supports. Restriction of movement was made on 6 degrees to restrict heaving, swaying, surging, pitching, yawning and rolling. Figure 17 shows an isometric view for the preparation of the restriction setup.

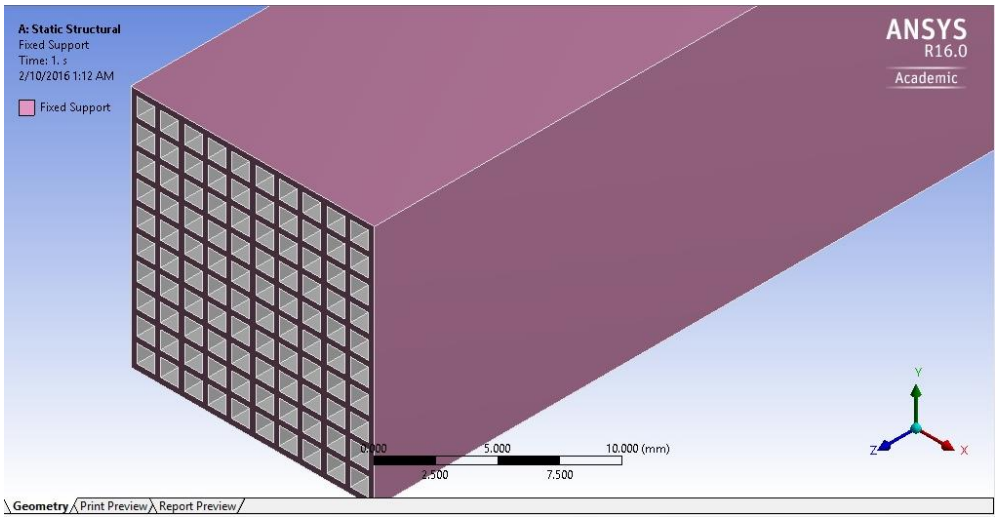

FIGURE 17: FIXED SUPPORTS IN PINK (3 FACES SHOWN)

Results show that the maximum deflection within the body is within the acceptable region. Figure 18 shows the scene deflection along with the minimum and maximum values in an actual value scale.

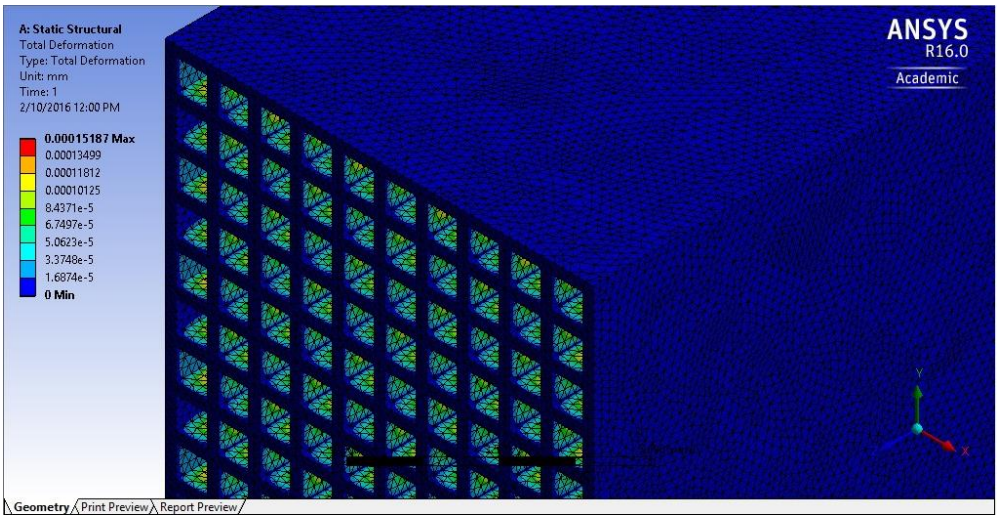

FIGURE 18: RESULTS OF TOTAL DEFORMATION ON THE CHANNELS (MM)

Figure 19 show that the maximum shear stress is on the walls of the HP fluid, with a maximum value of (37.6). It is noticed as expected that the maximum deflection happens at the walls of the high pressure channels. The normal stress (figure 20) on the geometry is also found, with a maximum value of (40.3) MPa.

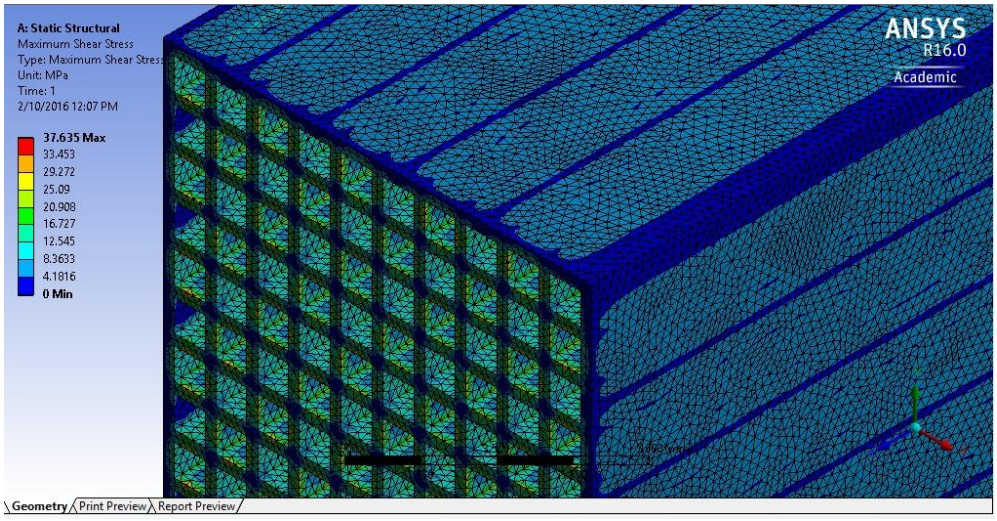

FIGURE 19: SHEAR STRESS (MPA)

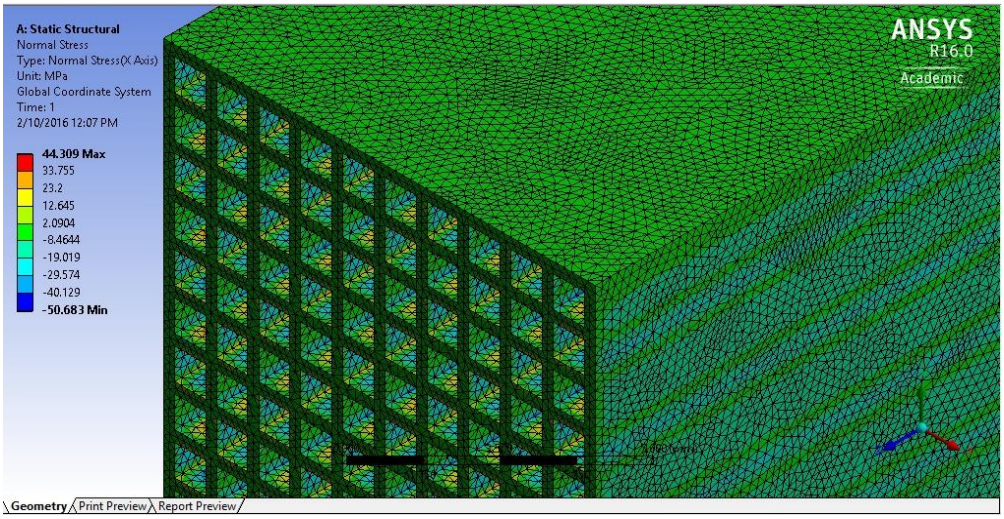

FIGURE 20: NORMAL STRESS (MPA)

FUTURE WORK

In future studies, field functions for pressure of the working fluid along the entire length and material temperature will be considered to calculate thermal stresses. Headers of the MCHE will also go through a CFD analysis to evaluate pressure losses.

CONCLUSION

Microchannel heat exchangers can be the key to increasing the overall efficiency of a recompression recuperated cycle. This paper suggests the design and analysis of a high and low temperature heat exchangers that can be used in a 100MW net power RRC S-CO2 Brayton cycle power system, with an overall efficiency of 59.11%. The use of Polymer Derived Ceramic Composite as a class of material is discussed along with the

manufacturing process. The finite enthalpy method is used to mathematically model and discretize both heat exchangers. The maximum pressure of 24MPa on the inner walls is a challenge for the overall structural integrity and therefore, a structural analysis is done on the low temperature recuperator and the results indicate a statically stable geometry.

NOMENCLATURE

D_h	Hydraulic Diameter (m)
E	Young's Modulus
f_D	Friction Factor
FHM	Finite Enthalpy Method
GA	Genetic Algorithm
h	Specific Enthalpy ($\frac{kJ}{kg.K}$.)
h_{conv}	Heat Transfer Coefficient ($^{W}/_{m^2.K}$)
HP	High Pressure
HRSG	Heat Recovery Steam Generator
HTR	High Temperature Recuperator
t	Channel Wall Thickness
k	Thermal Conductivity ($^{W}/_{m.K}$)
$LMTD$	Log Mean Temperature Difference
LP	Low Pressure
LTR	Low Temperature Recuperator
$\dot{m}$	Mass Flow Rate (kg/s)
MCHE	Microchannel Heat Exchanger
n	Number of
Nu	Nusselt Number
P	Pressure
PDCC	Polymer Driven Ceramic Compound
$P_{HP_{in}}$	Inlet Pressure of HP Fluid
PIP	Polymer Infiltration and Pyrolysis
Pr	Prandlt Number
$\dot{Q}$	Heat Load (W)
R	Thermal Resistance ($^{K}/_{W}$)
Re	Reynolds Number
RRC	Recompression Recuperated Cycle
S	Specific Entropy (kJ/kg)
S-CO2	Supercritical Carbon Dioxide
T	Temperature (K)
$T_{HP_{in}}$	Inlet Temperature of HP Fluid
V	Velocity (m/s)
W	Work (kJ/kg)

Greek

Δ	Difference
ε	Roughness (m)
ρ	Density ($^{kg}/_{m^3}$)

Subscript

c	Compressor
Conv.	Convection
e	Element
$frac$	Fraction of Mass Flow rate
H	Hydraulic
HP	High Pressure
LP	Low Pressure
t	Turbine

REFERENCES

[1] Feher E. G., "The Supercritical Thermodynamic Power Cycle", Douglas Paper No. 4348, presented to the IECEC, Miami Beach, Florida, August 13-17, (1967).

[2] Dostal, V., Driscoll, M.J., Hejzlar, P., 2004, "A Supercritical Carbon Dioxide Cycle for Next Generation Nuclear Reactors", MIT-ANP-TR-100.

[3] Colombo, P., Mera, G., Riedel, R. and Sorarù, G. D. (2010), Polymer-Derived Ceramics: 40 Years of Research and Innovation in Advanced Ceramics. Journal of the American Ceramic Society, 93: 1805–1837. doi:10.1111/j.1551-2916.2010.03876.x

[4] G. Mera and R. Riedel "Organosilicon-Based Polymers as Precursors for Ceramics"; pp. 51-89 in Polymer Derived Ceramics: From Nanostructure to Applications, Edited by P. Colombo, R. Riedel, G. D. Soraru, and H.-J Kleebe. DES

[5] Riedel R., Mera G., Hauser R., Klonczynski A., Silicon-Based Polymer-Derived Ceramics: Synthesis Properties and Applications-A Review Dedicated to Prof. Dr. Fritz Aldinger on the occasion of his 65th birthday. J ceram Soc

[6] Wang, K., Polymer Derived Ceramics: High Temperature Applications in Nanoscale

[7] Cox, S. B. (2004) Processing and Characterization of Continuous Basalt Fiber Reinforced Ceramic Matrix Composites Using Polymer Derived Ceramics, MsC thesis

[8] Ryu, H.-Y., Wang, Q. and Raj, R. (2010), Ultrahigh-Temperature Semiconductors Made from Polymer-Derived Ceramics. Journal of the American Ceramic Society, 93: 1668–1676. doi:10.1111/j.1551-2916.2010.03623.x

[9] P. A. Ramakrishnan, Y. T. Wang, D. Balzar, Linan An, C. Haluschka, R. Riedel and A. M. Hermann (2001), Silicoboron–carbonitride ceramics: A class of high-temperature, dopable electronic materials. American Institute of Physics

[10] Shao G. (2013), Development of Polymer Derived SiAlCn Ceramic and its Applications for High-Temperature Sensors, PhD Dissertation

[11] Mohagheghi, M., Kapat, J., “Thermodynamic Optimization of Recuperated S-CO2 Brayton Cycles for Solar Tower Applications”, proceedings of ASME Turbo Expo, San Antonio, Texas, June 3-7, (2013).

[12] Schmitt, J., Amos, D., Kapat, J., “Design and Real Fluid Modelling of Micro-channel Recuperators for a Nominal 100MW Class Recuperated Recompression Brayton Cycle Using Supercritical Carbon Dioxide”, Proceedings of ASME Turbo Expo, Montreal, Canada, June 15-19, (2015).

[13] Lemmon, E.W., Huber, M.L., McLinden, M.O., 2010, NIST Standard Reference Database 23: Reference Fluid Thermodynamics and Transport Properties-REFPROP”, Version 9.0, National Institute of Standards and Technology, Standard Reference Data Program, Gaithesburg.